Cylinder Pressure [bar]

100
90
80
70
60
50
40
30
20
10
0

-90   0

Pressure Sensors

Application of an Improved Model for the Determination of Acoustic Resonances in Indicator Passages for Combustion Pressure Measurements in Large Bore Gas Engines

Thomas Walter
Kistler Instruments AG
Winterthur, Switzerland

Christoph Gossweiler
University of Applied
Sciences North Western
Switzerland

Bryan Willson
Colorado State University
Fort Collins, Colorado USA

Pressure Sensors

Application of an Improved Model for the Determination of Acoustic Resonances in Indicator Passages for Combustion Pressure Measurements

Thomas Walter, Kistler Instruments AG, Winterthur, Switzerland
Christoph Gossweiler, University of Applied Sciences North Western, Switzerland
Bryan Willson, Colorado State University, Fort Collins, Colorado USA

Content

Pressure Sensors

Application of an Improved Model for the Determination of Acoustic Resonances in Indicator Passages for Combustion Pressure Measurements

Thomas Walter, Kistler Instruments AG, Winterthur, Switzerland
Christoph Gossweiler, University of Applied Sciences North Western, Switzerland
Bryan Willson, Colorado State University, Fort Collins, Colorado USA

1. Abstract

The acoustic resonances in indicator passages are often modeled using either a Helmholtz or a so called organ pipe acoustical model. However, in practice these models often indicate natural frequencies which are too high.

This paper proposes the Bergh and Tijdeman model [1] which is more accurate and which was originally developed for pressure measurements in turbomachinery. This paper presents the theoretical basis for the Berg / Tijdeman model and then uses it to explore signal distortion from a variety of indicator passage geometries. In order to validate the approach, a flush-mounted water-cooled Kistler reference transducer was used to measure accurate in-cylinder combustion data in an automotive Diesel engine. An additional sensor was recess mounted with passages of different geometries. The Bergh Tijdeman model was then applied to investigate the acoustic distortion of the indicator passages. The results show excellent agreement with the experimental data, which are much closer than using the Helmholtz or the organ pipe model.
Further the Bergh and Tijdeman model is applied to complex indicator passage geometries with multiple cavities. Again, for comparison, a flush-mounted Kistler reference transducer was used to measure accurate in-cylinder combustion data in a large-bore natural gas engine. Three additional sensors were mounted using different indicator passage geometries. The engine was operated under base line and knocking combustion conditions. The Bergh Tijdeman model was then applied to model the acoustic distortion of the three indicator passages and again showed good agreement with the experimental data.

Finally, the paper proposes simple rules for implementing indicator passages in large gas engines.

1.1 Introduction

Measuring combustion pressure is becoming increasingly more important due to pressure based engine management and closed loop combustion control systems. Piezoelectric sensors are the instrumentation of choice when performing engine combustion research and development. Recent adaptations of this technology to industrial environments have resulted in its successful application for combustion pressure monitoring of large bore gas engines. These small sensors have a large measuring range, high temperature accuracy and long-term stability. When installing a piezoelectric pressure sensor in a combustion chamber, the measured pressure values can be used for engine control. Especially when implemented on older engines, operation could be significantly improved, providing e.g. better efficiency, reduced emissions, and increased engine durability.

However, due to restrictions of accessing the combustion chamber or due to established engineering practices, the installation of sensors is not standardized and a large number of different sensor locations are currently used. Ideally for best accuracy, a combustion sensor should be flush-mounted in the combustion chamber, but often this is not possible and sensors must be installed recessed. In these cases, pressure from the combustion chamber travels through an indicator passage, to reach the sensor and signal acoustic oscillations and signal distortion can occur. These oscillations are superimposed on the combustion pressure affecting the signal quality and making important information like e.g. maximum pressure or knock intensities difficult to extract.

2. Physics of Acoustic Oscillations

Acoustic oscillations in indicator passages are stimulated by fast pressure fluctuations at the entrance of the passage. Due to the compressibility of the gas column in the cavity of the passage, the pressure fluctuation at the entrance of this cavity produces an excitation of the oscillation within the gas column. This pressure oscillation of the cavity is superimposed on the combustion pressure and the pressure sensor is sensing both pressures. Typically, the excitation of the acoustic oscillation is triggered by the fast pressure rise after the start of the combustion cycle.

Sensor Flush Mounted   Kistler Type 6061

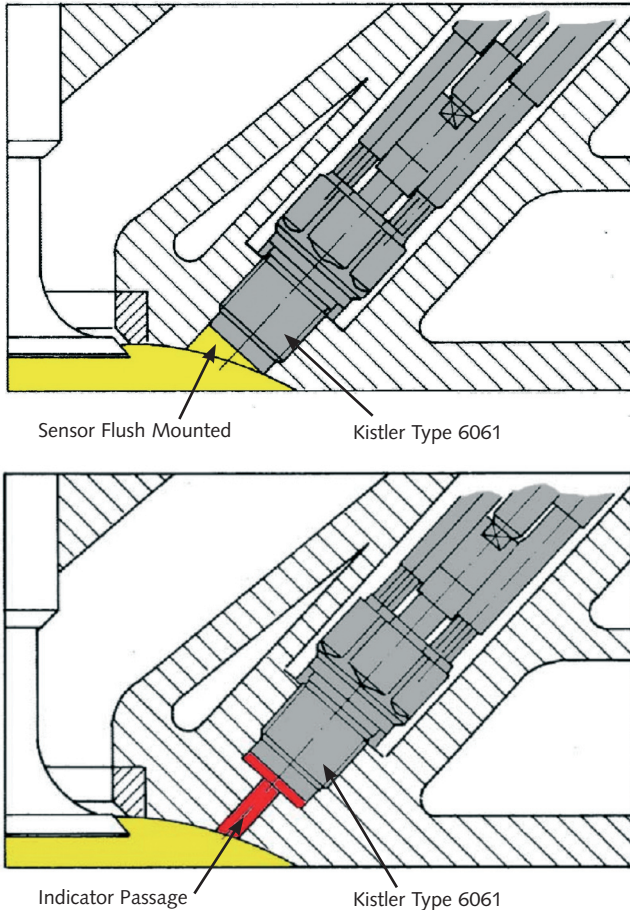Indicator Passage   Kistler Type 6061

Figure 1: Sensor flush mounted and recessed mounted. The indicator passage consists of a tube followed by a volume in front of the piezoelectric sensor.

Figure 2: Acoustic oscillations in an indicator passage. The fast pressure rise at the beginning of the combustion excites the oscillation.

Nomenclature

Variables:

A	[m²]	Area
c	[m/s]	Sonic speed
D	[m]	Diameter
F	[N]	Force
f	[Hz]	Frequency
H	[-]	Transfer function
J_n		Bessel function first kind, order n
j	[-]	imaginary unit
L	[m]	Dimension
m	[kg]	Mass
N	[-]	Number of tubes and volumes
P_r	[-]	Prandtl number
p	[Pa, bar]	Pressure
R	[J/kg K]	Gas constant
T	[K]	Temperature
u	[m/s]	Speed
V	[m³]	Volume
x	[m]	Displacement
κ	[-]	Ratio of specific heats
λ	[m]	Wave length
ρ	[kg/m³]	Fluid density
ω	[rad/s]	Frequency variable

Indices:

T	Tube
C	Cavity
n	Natural

A typical cylinder pressure trace of sensors using such an indicator passage is shown in Figure 2. Around the maximum pressure, the combustion pressure curve shows an acoustic oscillation with a frequency of about 6 kHz and amplitudes of about ± 6 bar.

This resonance frequency of 6 kHz distorts all pressure signals above about 4 kHz and also affects the accurate detection of the maximum pressure.

When a sensor installation requires an indicator passage, it is necessary to model the natural frequency of the indicator passage accurately and to design the size and shape of the passage to optimize the signal quality.
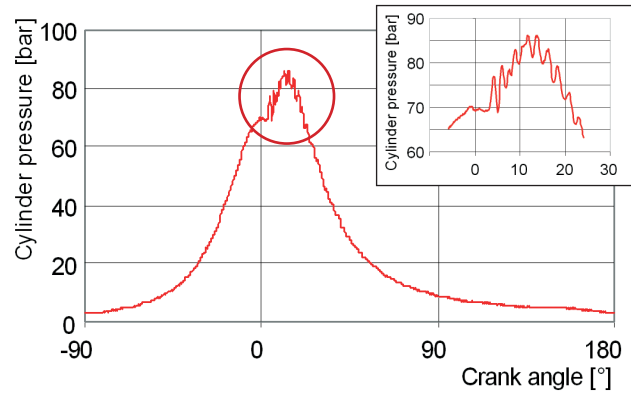
2.1 Modelling of Indicator Passages

For modeling indicator passages the equation of the Helmholtz resonator and the organ pipe resonance are commonly used. As a third model the method of Bergh, Tijdeman [1] is shown.

2.1.1 Natural Frequency of the Helmholtz Resonator

The model of the Helmholtz resonator (Fig. 3) considers the resonating cavity as a spring / mass model. The gas in the cavity volume V_c acts as a spring and the gas in the tube is considered as the mass m_T (lumped parameter model). By applying Newton's law and assuming the pressure being uniform inside the cavity:

$$F = m_T \cdot \frac{d^2x}{dt^2} = A_T \cdot dp = A_T \cdot \Delta V \frac{dp}{dV_C} = A_T \cdot A_T \cdot x \cdot \frac{dp}{dV_C} \quad (1)$$

with the adiabatic bulk modulus

$$-V \cdot \frac{dp}{dV} = \rho \cdot \kappa \quad (2)$$

and $m_T = p\, A_T\, L_T$, the differential equation results

$$\frac{d^2x}{dt^2} + \frac{A_T \cdot \kappa \cdot \rho}{V_C \cdot \rho \cdot L_T} x = 0. \quad (3)$$

For harmonic motion the natural frequency fn can be calculated and the Helmholtz equation results:

$$f_n = \frac{c}{2\pi} \sqrt{\frac{A_T}{V_C \cdot L_T}} \quad (4)$$

with c being the sonic speed. For an ideal gas c is:

$$c = \sqrt{\kappa \cdot R \cdot T} \quad (5)$$

Due to the assumption that the pressure is uniform inside the cavity, the important condition for the wave length l of the sound wave results:

$$\lambda_H = \frac{c}{f_n} \gg L_H \quad (6)$$

where L_H is the length of the Helmholtz resonator. This condition results to quite large volumes, producing relatively low natural frequencies. Such configurations should be avoided for indicator passages. Further on, in the derivation of the Helmholtz equation it was assumed that the mass consists of the gas in the tube. Due to the in – and outflow of the gas an additional mass portion oscillates. Therefore, depending on the dimensions of the resonator the natural frequency calculated proves to be too high. For such geometries a length correction term ΔL for added mass is included and $L_{eff} = L_H + \Delta L$ is used to calculate the natural frequency (Junger [2]). For small tube diameters compared to the cavity diameter, ΔL is set to $\Delta L \approx 0.48\, A_T^{1/2}$.
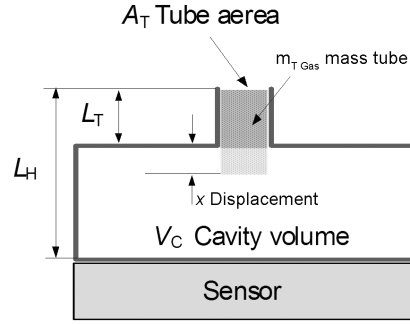

Figure 3: Helmholtz resonator

2.1.2 Natural Frequency of a Prismatic Tube

Often, indicator passages are formed as cylindrical tubes with one side open to the combustion chamber with the sensor mounted at the closed end. In these tubes an organ pipe resonance occurs, where a standing wave with the following boundary condition establishes (distributed parameter model):
Inlet:
pressure oscillation $p_{osc} = 0$; speed of oscillating fluid $u = u_{max}$
End, (sensor):
pressure oscillation $p_{osc} = p_{osc,\,max}$; speed of fluid $u = 0$.
Therefore in the cylindrical tube, the pressure oscillation varies along the tube with maximum oscillation amplitude at the sensor location.
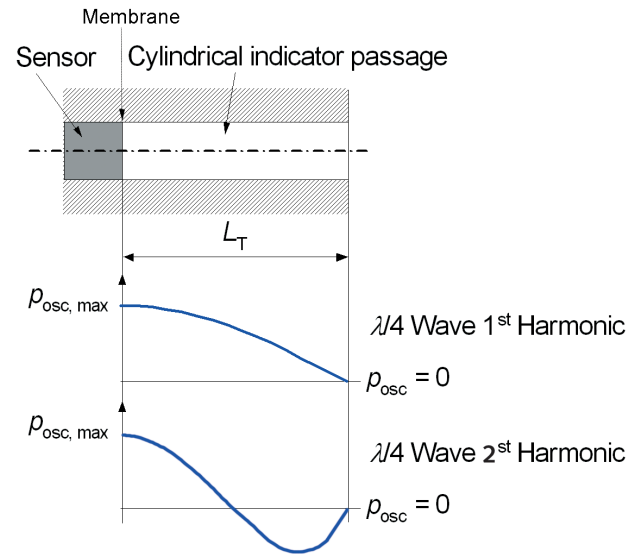

Figure 4: Standing wave in a prismatic tube (organ pipe resonance)

The first harmonic natural frequency of the organ pipe resonance is:

$$f_n = \frac{c}{4 \cdot L_T} \quad (7)$$

Again, due to the in – and outflow, added mass effects take place especially for short passages with respect to their diameter.

2.1.3 The Bergh and Tijdeman Model

For a multiple series of N connected tubes and volumes, Bergh and Tijdeman [1] derived a general recursion formula that calculates the transfer function H of volume i and therefore relates the pressure disturbance in preceding volume i-1 and the next volume i+1.
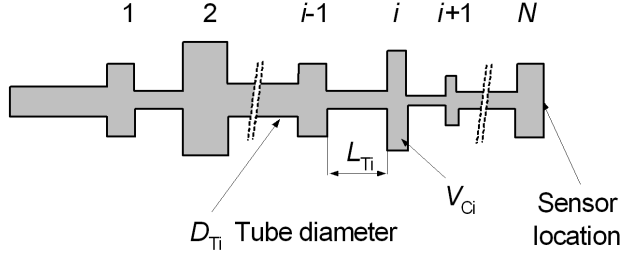

Figure 5: Bergh & Tijdeman model: system of N tubes and cavities

By using the Navier-Stokes equation, the energy equation and the equation of continuity, a system of coupled differential equations was derived and simplified by assuming that:

• the sinusoidal pressure disturbances are small
• the diameter of the tube is small compared to its length
• the ideal gas equation is valid
• the flow is laminar throughout the system

By solving these differential equations the complex transfer function $H_i = p_i / p_{i-1}$ results. The transfer function of volume i relates the pressure fluctuation of volume i-1 and i+1:

$$\frac{p_i}{p_{i-1}} \left[\cosh \langle \o_i L_{Ti} \rangle + \frac{V_{ci}}{V_{Ti}} \left(\sigma_j + \frac{1}{k_i} \right) n_i \o_i L_{Ti} \sinh \langle \o_i L_{Ti} \rangle + \right.$$

$$\frac{V_{Ti+1} \o_{i+1} L_{Ti} J_0 \langle \alpha_i \rangle J_2 \langle \alpha_{i+1} \rangle}{V_{Ti} \o_i L_{Ti+1} J_0 \langle \alpha_{i+1} \rangle J_2 \langle \alpha_i \rangle} \frac{\sinh \langle \o_i L_i \rangle}{\sinh \langle \o_{i+1} L_{i+1} \rangle}$$

$$\left. \left\{ \cosh \langle \o_{i+1} L_{i+1} \rangle - \frac{p_{i+1}}{p_i} \right\} \right]^{-1}$$

$$\o = \frac{\omega}{c} \cdot \sqrt{\frac{J_0 \langle \alpha_i \rangle}{J_2 \langle \alpha_i \rangle}} \sqrt{\frac{\kappa}{n_i}}$$

with:

$$\alpha_i = j \sqrt{j} \; \frac{D_{Ti}}{2} \; \sqrt{\frac{p_i f}{\mu_i}} \quad \text{(so called shear wave number)}$$

$$n_i = 1 + \left[\frac{\kappa - 1}{\kappa} \frac{J_2 \langle \alpha_i \sqrt{P_r} \rangle}{J_0 \langle \alpha_i \sqrt{P_r} \rangle} \right]^{-1}$$

J_n		Bessel function first kind, order n
j		Imaginary unit
P_r	[-]	Prandtl number
ρ	[kg/m³]	Fluid density
ω	[rad/s]	Frequency variable
σ_j	[-]	Relative volume increase due to sensor diaphragm deflection (to be neglected for piezoelectric sensors)

With equation (8) the transfer functions of the volumes 1 to N are calculated. By multiplying these complex transfer functions the over all transfer function H_{1-N} from inlet (1) to Sensor (N) results. The absolute value (amplitude ratio) and the argument (phase) of the transfer function can be diagramed in a Bode plot. As an example the Bode plot of an indicator bore with $L_T = 5$ mm, $D_T = 3,3$ mm, $V_c = 70$ mm³ is shown in Figure 6. The calculated natural frequency of $f_n = 18,9$ kHz is in excellent agreement with an actual measurement in a Diesel engine showing $f_n = 18,5$ kHz.
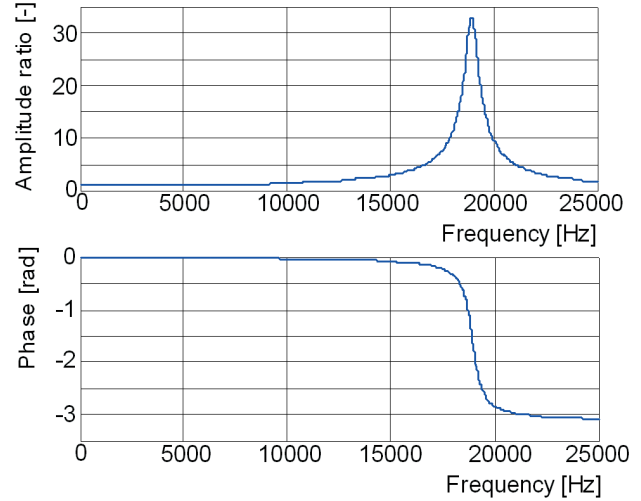

Figure 6: Transfer function (Bode plot) of a indicator passage ($L_T = 5$ mm, $D_T = 3,3$ mm, $V_c = 70$ mm³) calculated with equation (8)

2.2 Experiment for Validation

Validation experiments have been conducted by Schnepf [3] in a pre-chamber 5-cylinder Diesel engine MB 201 with a displacement of 2,5 l. A water-cooled Kistler sensor Type 6061 with an M10 thread was mounted in an adapter that allowed the indicator passage to be varied. The dimensions of the indicator bore of the adapter were $D_T = 5,0$ mm, $V_c = 80$ mm³. The tube length was adjustable from $L_T = 5$ mm to $L_T = 50$ mm. The pipe oscillations were clearly visible in the cylinder pressure signals. The resonant frequency was analyzed by means of power spectral density calculations. In Figure 7 the experimental data of Schnepf [3] are compared to calculated natural frequencies with the three models listed above. For the calculation of the speed of sound an accurate determination of the ratio of specific heats κ and the gas temperature is necessary. Since no combustion takes place in the indicator passage, the ratio of specific heats is set to the value measured for the engine during the compression stroke $\kappa = 1,38$. For the gas temperature, the adiabatic temperature, depending on the pressure ratio and the gas temperature in the passage at the beginning of the compression stroke can be set. For his validation experiments, Schnepf [3] determined the gas temperature to be $T = 970$ K.
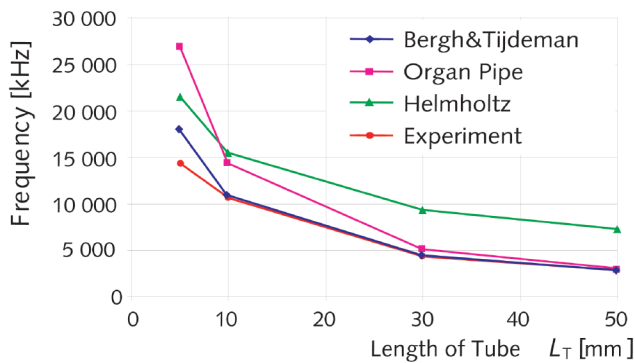
Figure 7: Comparison of measured resonance frequencies to the calculated values. The Bergh & Tijdeman model shows the best agreement to the experimental data

From Figure 7 it can be concluded that:

- For long tubes where $L_T/D_T \gg 1$, the agreement of the organ pipe model and the Bergh & Tijdeman approach with the experimental data is excellent.
- The smaller the ratio L_T/D_T the larger the deviation between the organ pipe model and the experimental data. Since a tiny cavity volume of $V_c = 80$ mm³ is present at the sensor, the organ pipe model delivers no valid data since it considers the tube to be prismatic without any additional cavities. For purely prismatic tubes without any additional cavity volume the organ pipe model is able to predict the natural frequency with good accuracy for ratios $L_T/D_T > 1$. For smaller ratios of L_T/D_T an added mass correction becomes important.
- The Helmholtz equation shows a natural frequency which is too high and therefore is not applicable for such geometries. Since the cavity volume of the indicator passages is kept as small as possible in order to reach the highest natural frequency, the important condition (6) is not fulfilled. The pressure over the indicator passage is not uniform and the lumped parameter spring / mass model of the Helmholtz resonator fails completely in these applications.
- The Bergh and Tijdeman model shows excellent agreement with the experimental data for ratios $L_T/D_T > 2$. For shorter tubes, the added mass effect becomes important, leading to larger deviations. Additional validation experiments, using an aerodynamic shock tube, proved that the Bergh and Tijdeman model is able to predict the natural frequencies of a multitude of passage geometries with excellent accuracy (Planta [4]).

3. Installation of Combustion Pressure Sensors in Large Bore Gas Engines

The majority of the pressure sensors used on large bore gas engines are installed in indicator valves. These indicator valves represent the traditional access to the combustion chamber and they have the following advantages:

- uses existing and standardized bore to the combustion chamber
- sensor is easy to install
- sensor can be exchanged under running conditions
- widely used in the U.S. Gas Pipeline industry.

However there are also two significant disadvantages:

- the large bores and cavities between the sensor and the combustion chamber cause acoustic resonances
- the indicator valve has only limited capabilities for heat dissipation and expose the sensor to high temperatures.

The bores and cavities between the sensor and the combustion chamber cause resonances which limit the bandwidth of the dynamic signal to be measured and therefore limit the ability to detect knocking or detonating conditions. This situation is even more crucial as CLCC-Systems (Closed Loop Combustion Control) are gaining on importance for engine management systems.

To investigate the indicator passage resonances, a cylinder head of a 4-cylinder Cooper GMV Engine was specially prepared to allow simultaneous pressure measurements at four different locations on cylinder head number 4. As shown in Figures 8 and 9, the four sensor locations include a reference position with a flush mounted sensor in the combustion chamber (position 1) and three typical installation positions widely found in the field (positions 2 ... 4).

Position	Path Length [mm/"]		Sensor Type
Position 1	0 mm, (Flush mount)		Kistler 6613C2
Position 2	172 mm	6.772"	Kistler 6613C2
Position 3	182 mm	7.165"	Kistler 6613C2
Position 4	521 mm	20.512"	Kistler 6613C2

Table 1: Indicator passages 1 ... 4 , path length and sensors installed

Kistler Sensor Type 6613C2

Thread Size [–]	M10
Pressure Range [psi / bar]	1 500/103
Max. Temperature [°C]	350
Charge Amplifier	integrated
Sensitivity [mV/bar]	10.00
Thermal Shock [bar]	±0.5
Natural Frequency [kHz]	90
Lifetime [h]	16 000

Figure 8a: Pressure sensor Kistler Type 6613C2, for monitoring applications on large bore gas engines

Position 2
Sensor installed in
Indicator Valve

Position 1
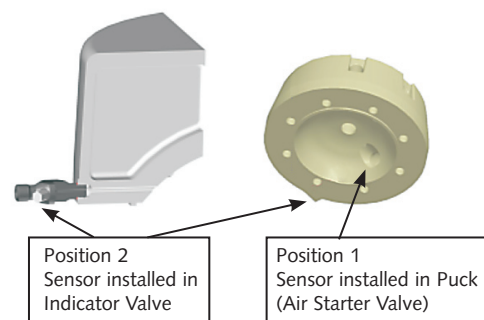Sensor installed in Puck
(Air Starter Valve)

Figure 8b: Indicator passages positions 1 and 2
Position 1: reference sensor with a flush mounted piezoelectric Kistler Type 6613C2
Position 2: sensor Type 6613C2 mounted in indicator valve

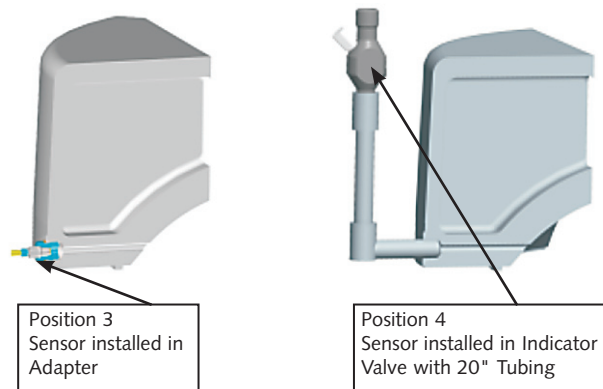| Position 3	Position 4
Sensor installed in Adapter	Sensor installed in Indicator Valve with 20" Tubing

Figure 8c: Indicator passages positions 3 and 4 with piezoelectric sensors for combustion pressure monitoring (Kistler Type 6613C2)
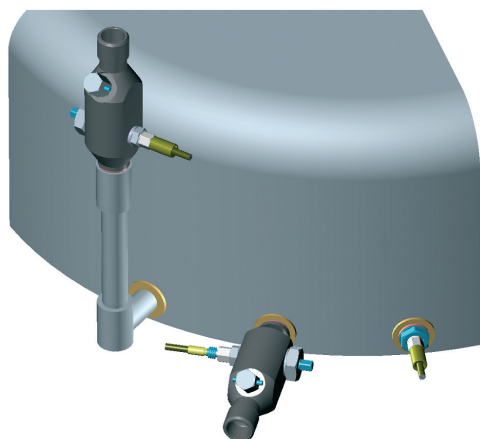

Figure 9: Indicator passage locations Pos. 2 ... 4 on the cylinder head

3.1 Calculated Natural Frequencies for Positions 1 to 4

To determine the natural frequency of indicator valves using equation (8), the passage has to be divided up and simplified to a series of tubes and cavities. The accurate modeling is important especially for large volumes found in indicator valves, adapters and conical thread joints (Figure 10). Since the Bergh and Tijdeman model is a one dimensional model, 3-D effects like e. g. bends (Pos. 4) can not be modeled. It has been proven by means of shock tube experiments that bends would not influence the natural frequency predictions of the most important lower harmonics.

To calculate the sonic speed, the ratio of specific heats and the gas temperature are set to $\kappa = 1{,}38$ and $T = 800$ K. Under normal operating conditions in gas engines, no combustion takes place in the indicator bore. Therefore the adiabatic gas temperature can be used to calculate the speed of sound.
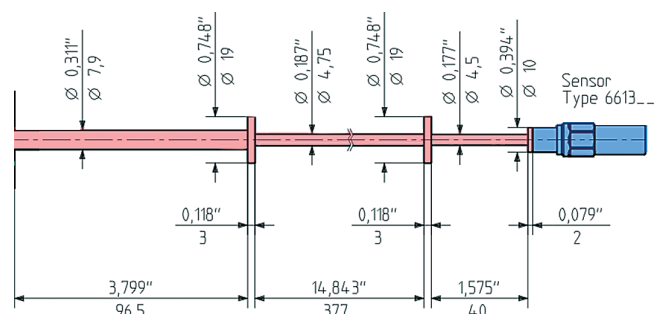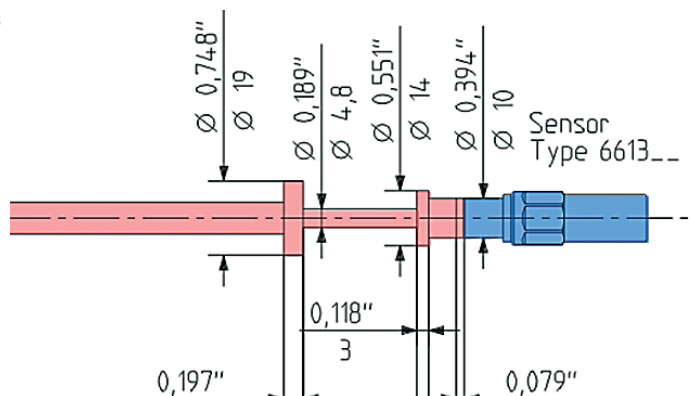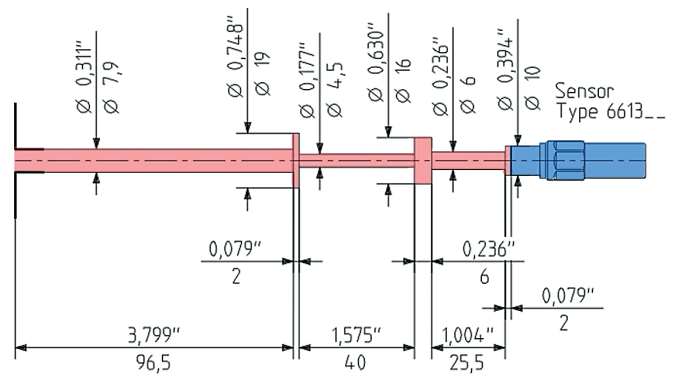

Figure 10: Tube / volume models of the indicator passages 2 (top), 3 (middle) and 4 (bottom)

The amplitude ratio calculated is shown in Figure 11.

The passage at position 3, with the short path length and the smallest cavity volumes, generates the largest amplitude ratio with the highest first natural frequency. Position 4 represents the longest path length of the passages with the smallest amplitude ratio with the lowest first natural frequency. The reason for this is the damping effect of the oscillating flow process (breathing) over a working cycle in the large tubes and cavities. The straight tube with the small cavity volume at position 3 leads to significantly higher oscillation amplitudes due to low damping.
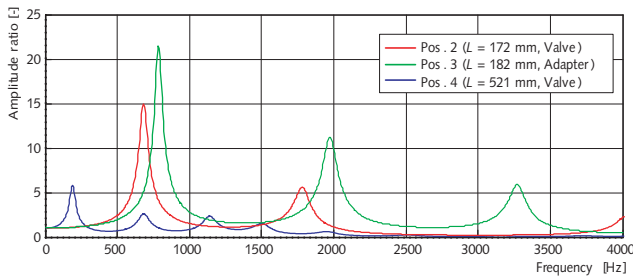
Figure 11: Amplitude ratios for the indicator passages Pos. 2, 3, 4, calclated with the Bergh and Tijdeman model

Table 4 shows a summary of the resulting first and second harmonics, as well as the maximum frequency bandwidth which could be reliably detected. As a role of thumb the useful maximum frequency bandwidth can be approximately 50 % of the resonance frequency (3 dB amplitude ratio).

Cylinder / Position	1st Natural Frequency	2nd Natural Frequency	Maximum detectable Frequency
Position 2	675 Hz	1770 Hz	337 Hz
Position 3	785 Hz	1975 Hz	392 H
Position 4	185 Hz	675 Hz	92 Hz

Table 2: First and second harmonics of the indicator passages at Pos. 1 ... 4 calculated with the Bergh and Tijdeman model

4. Test Program and Results
4.1 Engine Specification and Load Conditions
All testing was done at the Energy Conversion Laboratory at the Colorado State University on a 4-cylinder Cooper GMV Engine. Measurements were taken at rated speed/load under the following conditions:

• baseline (regular combustion conditions)
• knocking/detonating conditions

Knocking was accomplished by advancing the ignition timing and enriching the mixture until a clear knocking combustion could be heard. Since knocking operation of these kinds of engines are rather risky and dangerous, the engine could be run only for limited periods of time under these adverse conditions. For this reason it was not always possible to reach fully stabilized engine conditions and the results presented should only be used as relative and comparative data.
All data were collected unfiltered (12 bit resolution) and evaluated with a DSP ACAP System.

Specifications of Engine:

Engine Type	Cooper GMV
Bore [" / mm]	14 / 350
Stroke [" / mm]	14 / 350
Displacement [cid / L]	2154 / 33,7
Rated speed [rpm]	300
Rated load [HP / kW]	450 / 334
IMEP [psi / bar]	90 / 6,2 (baseline)

5. Results
5.1 Measured Pressure Signals at Different Sensor Locations
Figures 12 and 13 show the cylinder pressures versus crank angle of a typical, single combustion event at base line operation and at knock operation simultaneously measured at position 1 (flush mounted reference sensor) and at positions 2 to 4. Additionally the trace of the pressure difference between the reference cylinder pressures at position 1 and the pressure at the respective position (Dp_{x-1}) is added.

Pressure oscillations are clearly visible in the pressure difference plots under base line operation (Figure 12, cylinder pressure vs. crank angle). They occur at the start of combustion (position 2 to 4) which takes place around 185 °CA (5 °CA after TDC). The amplitudes of these pressure fluctuations are about ± 0,5 bar at pos. 2 and 3, and about ± 2,5 bar at position 4. Furthermore, the phase shift (see Figure 6) caused by the indicator passage produces a lag which is clearly visible in the pressure difference curve. This pressure lag is very obvious for position 4 where it results in a –2,5 bar error (see last two plots in Figure 12, where an additional full engine cycle is shown).

When operating under knocking conditions we find similar results. As shown in Figure 13, the start of combustion, which here takes place at around 175 °CA (5 °CA before TDC), also triggers some pressure oscillations, but with much larger amplitudes. The largest pressure oscillations are found at position 3 with amplitudes of almost ± 15 bar. This phenomenon is discussed later.

The corresponding amplitudes at position 2 and 4 are much smaller. Due to higher combustion pressures, the pressure lag of position 4 is also larger and is even larger than the associated pressure oscillation.
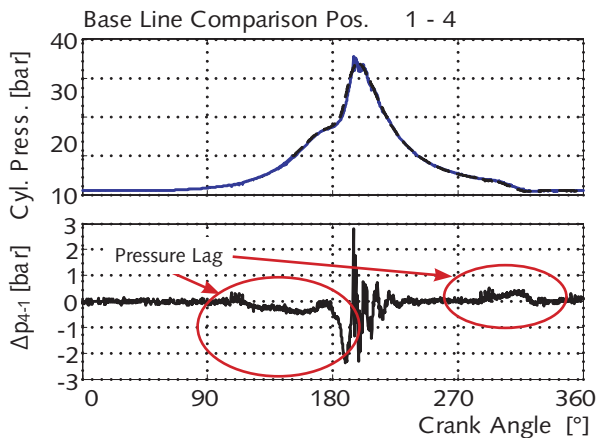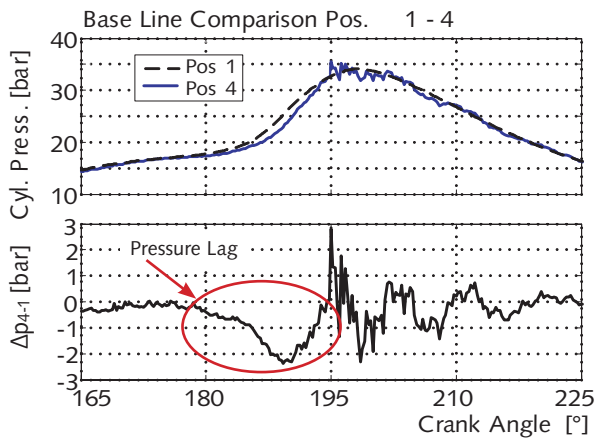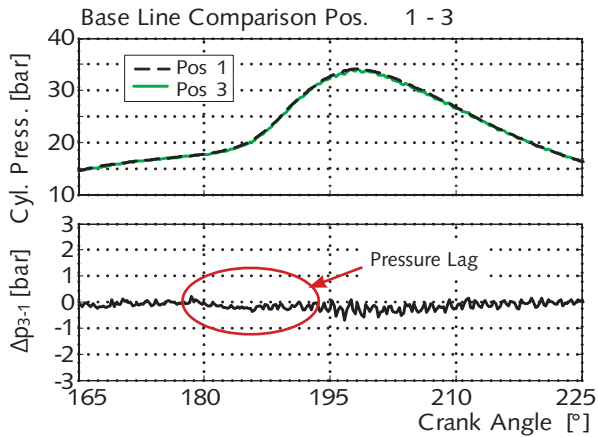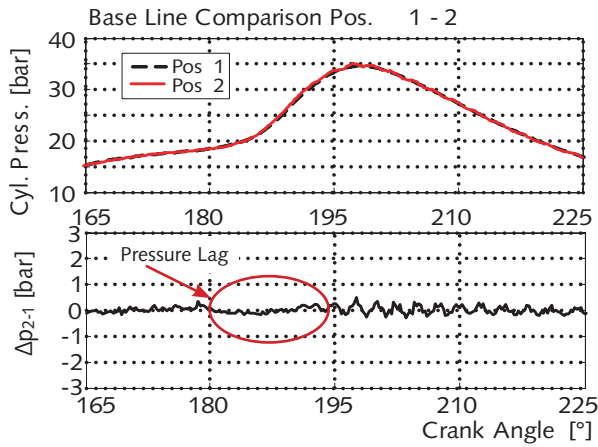
Figure 12: Comparison of cylinder pressure (base line). For Pos. 4 an additional full engine cycle is shown
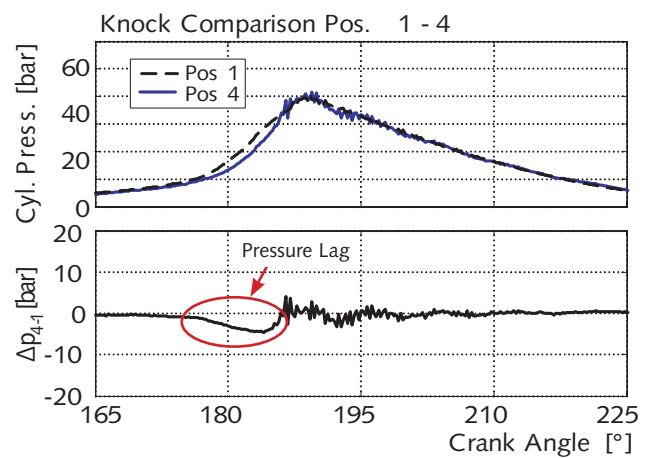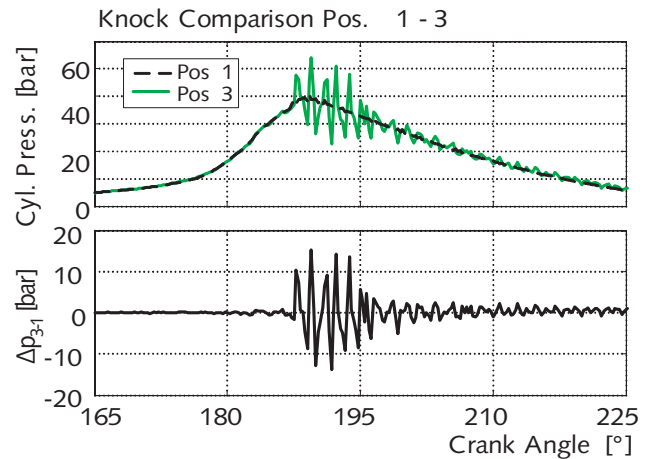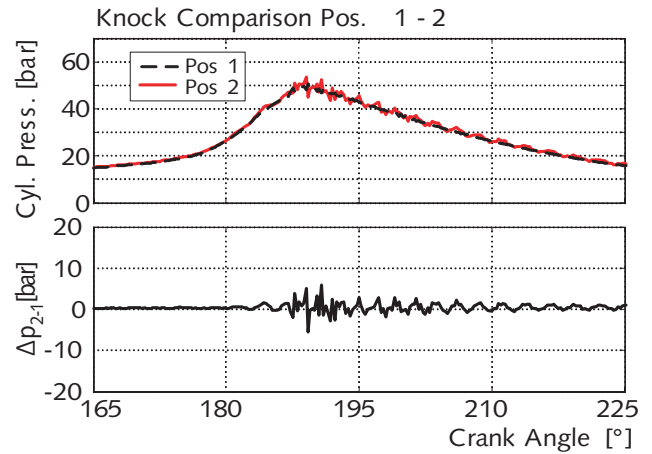

Figure 13: Comparison of cylinder pressure at different sensor locations at knock operation

5.2 Comparison of Experimental Results with Calculated Natural Frequencies

Figure 14 show the amplitude ratios calculated (as given in Figure 11) and the measured frequency spectra of the pressure signals for the sensor at position 2 to position 4 at base line testing. The measured spectra are scaled as sound pressure spectra where the ordinate is scaled to sound pressure level $L_p = 20 \log p/p_0$ [dB] ($p_0 = 2*10^{-5}$ N/m², international reference value for sound pressure level).

The spectrum of the reference location Pos. 1 (flush mounted in combustion chamber) shows an almost undisturbed trace without any significant resonances. Only at about 600 Hz and 1300 Hz, some scattering is noticeable, which is most likely caused by combustion chamber resonances.
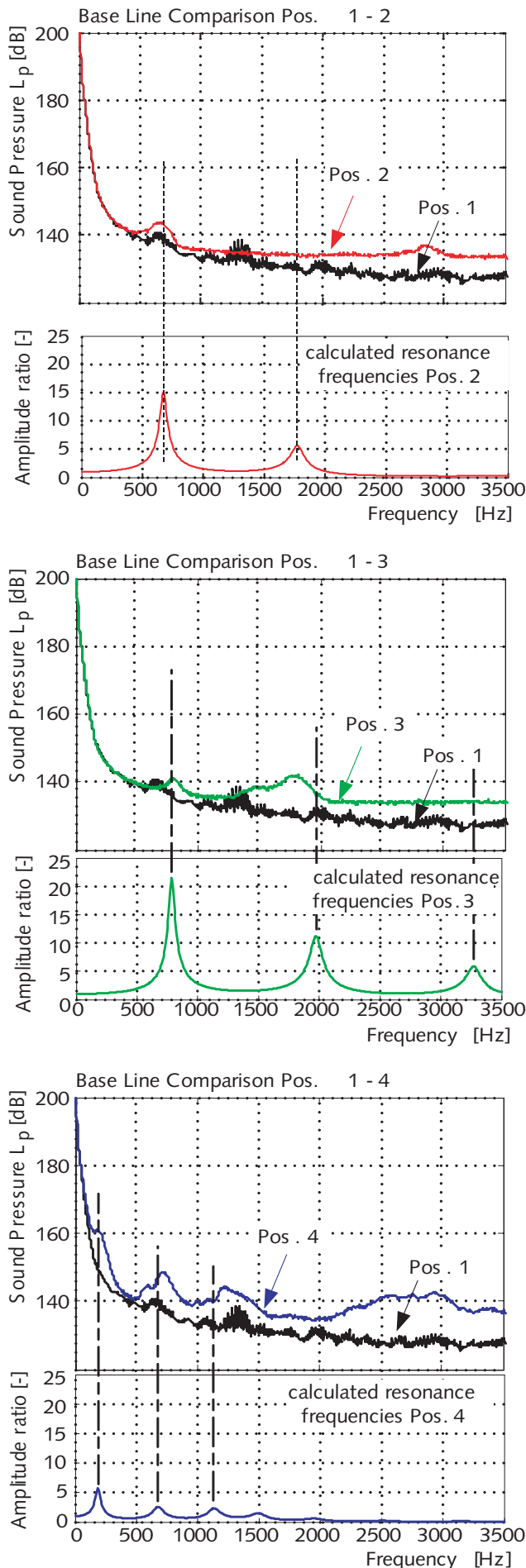
At position 2, a first resonance can be detected around 650 Hz, which reflects the resonance frequency of the indicator passage which corresponds well with the calculated results. However, the second resonance frequency at 2800 Hz does not correspond well with the calculated value of 1770 Hz. This is most likely due to the fact that the model of the cavities yields uncertainties in the determination of the dimension of tubes and associated volumes. This is especially true in the conical threads and the indicator valve. A major influence on the result has the gas temperature distribution. For simplification the temperature was set to a constant value of $T = 800$ K for the calculations.

The spectra at position 3 show a first resonance at about 800 Hz and a second resonance at about 1800 Hz. Both values correspond reasonable well with the calculations. Finally at position 4 the resonance frequencies are at about 200 Hz, 700 Hz and 1200 Hz, which is almost in perfect correlation with the calculated values. Over all it can be stated, that for the base line operation of the engine; the calculated natural frequencies are in good correspondence with the measured resonances.

Figure 15 shows the sound pressure spectra at knocking engine operation measured for the sensor locations Pos. 2 to 4. Observing the measured frequency spectra of the reference sensor position 1, there are additional significant peaks at about 1900 Hz and 2850 Hz with large amplitudes. These peaks are representing the pressure fluctuations which are induced by the knocking combustion and are very specific for the detection of a knocking combustion. The fact that the pressure levels in the high frequency region of the spectra are lower for position 1 is most likely caused by the different locations in the combustion chamber. While the indicator bores for position 2 to position 4 are close together at the cylinder liner, position 1 is located closer to the center of the combustion chamber. For knocking frequencies, the pressure level of the oscillation depends strongly on the location in the chamber (Walter et al. [5]).

Due to higher peak pressures under knocking condition, the sound pressure levels of the measured frequency spectra are generally higher than at base line operation. Comparing the measured and the calculated resonance frequencies at position 2 and 3, we find that the measured frequencies are slightly shifted towards higher values. This is most likely caused by the higher temperature level in these locations, which has not been taken into account in the calculations. At position 4, this frequency shift is of lower significance because the temperature variations in the long cavities are smaller for different operation modes of the engine. In the comparison of Pos. 1 and 3, we find also the reason for the large pressure fluctuations as seen in Figure 13. The natural frequency of this location is very close to the frequency of the pressure fluctuations caused by the knocking combustion. If knocking combustion occurs, the gas in the indicator passage of position 3 is in resonance and a 'perfect' oscillation with huge amplitudes can be detected.

Figure 14: Frequency spectra of pressure signals under base line engine operation
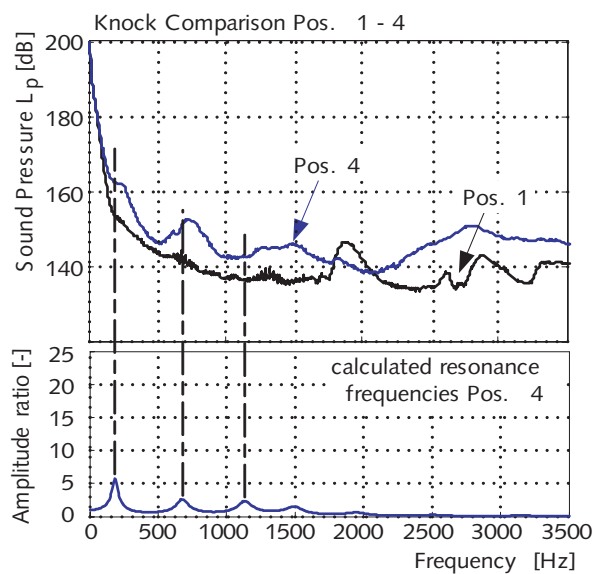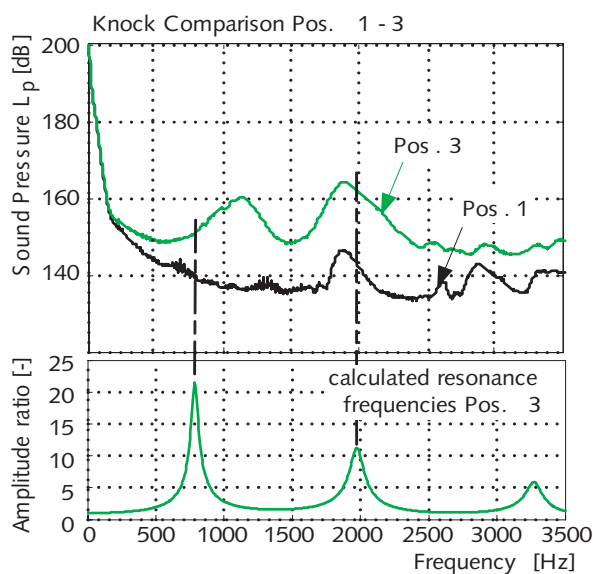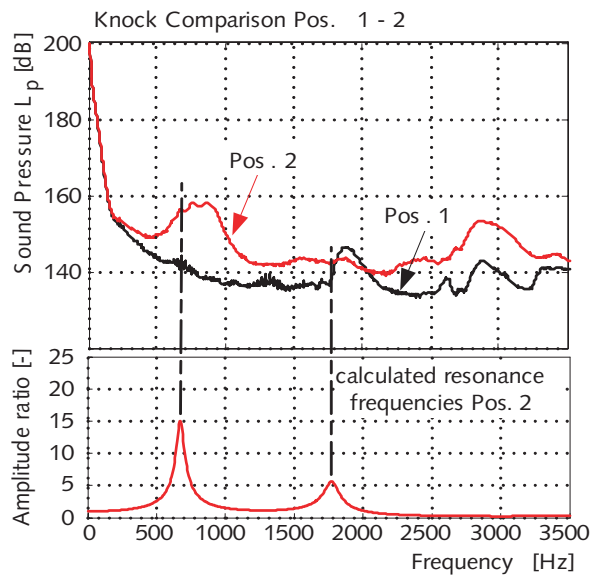
Figure 15: Frequency spectra of pressure signals at sensor locations Pos. 2 ... 4, under knocking engine operation

In general, there is a clear indication, that the applied model of calculating the acoustic oscillations in engines is also valid and applicable for knocking combustion.

Under knocking conditions, cylinder pressure signals clearly show that acoustic oscillations, superimposed on the combustion pressure affect the signal quality severely. Important information for engine monitoring or CLCC like e.g. maximum pressure or knock intensities can't be extracted out of such pressure traces. The long bores, often part of indicator valves, are not suitable to transmit signals with higher frequency content correctly. If high frequency information of the combustion process is needed, the geometry of the indicator passages has to be designed accordingly.

6. Recommendations for Sensor Installation in Large Bore Engines

Flush mounted sensor installation allows for the highest bandwidth of the signals without dynamic errors. This is especially important when using piezoelectric sensors that are unique with their natural high natural frequency. If a recessed installation of the pressure sensor has to be selected, certain requirements for diameter and length of the associated indicator passages have to be fulfilled. Figure 16, shows a diagram with achievable natural frequencies as a function of diameter and length of the indicator passage. Assuming that these gas engines have a minimum knock frequency of about 2 000 Hz, the natural frequency of the passage acoustic oscillation should be above 3 000 Hz. According to Figure 16, a passage with a diameter of $D_T = 5$ mm the maximum length of the tube is $L_T = 30$ mm, whereas passage with a diameter of 2,5 mm will not allow the minimum frequency to be measured. For monitoring knocking conditions shorter bores are recommended.
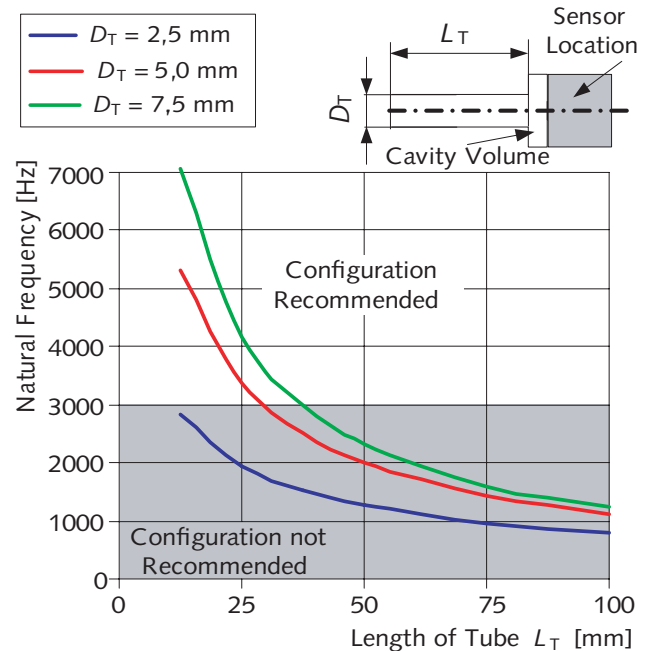

Figure 16: Indicator passage dimensions optimized for Kistler Type 6613 piezoelectric sensor. (Sensor passage dimensions according to Kistler Type 6613 data sheet). The natural frequencies were calculated with the Bergh and Tijdeman model

For an optimal sensor installation, the sensor temperature during operation has to be taken into consideration as well. Flush mounted installation of sensors in the combustion chamber allows the highest bandwidth of the frequency signals to be extracted from the combustion process. However, this location exposes the sensor to higher temperatures and requires good thermal contact with the cooled engine head. If pucks or insets are used for sensor installation, it is important that the puck fits tightly and that the material has good heat conductivity. A large sealing surface helps for a good heat transfer to the cooled engine head.

Installing the sensor directly in the cylinder head (similar position 3), provides a good heat transfer for the sensor and keeps the sensor temperature low. However, depending on the required frequency range of the cylinder pressure signal, the geometry of the indicator passage has to comply with the requirements for diameter and length, as presented in Figure 16.

If sensors are installed in indicator valves, it is important that the indicator valve is installed directly in the cylinder head and close to the cooling water jacket to assure for sufficient heat transfer. However, this installation is not suitable for measuring the higher frequencies of the pressure signal and is only recommended for low speed engines.

Sensor installations in indicator valves connected via an elbow tube are the least desirable locations. Not only is the bandwidth of the frequency signal extremely limited, but the thermal load of the sensor, especially under knocking conditions, could be very high and could overheat the sensor.

7. Summary and Conclusions

Three models for the determination of acoustic oscillations in indicator passages of combustion engines have been examined. It has been proven that, for typical geometries of indicator passages the Helmholtz model overestimates the natural frequency considerably. For this model the assumption that the wave length is much larger than the passage dimension (6) is not fulfilled.

The so called organ pipe acoustical model is able to predict the natural frequency of purely prismatic bores accurately. However, since indicator passages most often include at least one additional cavity, this model can't be applied for such geometries.

The most accurate results are achieved by using the Bergh and Tijdeman model. It has been shown that it can be applied successfully to predict the transfer function of complex indicator passages composed of multiple tubes and cavities.

When implementing indicator passages in large-bore natural gas engines the length of the passage and the cavity volume in front of the sensor should be as small as possible to allow for high frequency measurements. In typical monitoring configurations of large bore gas engines, piezoelectric sensors Kistler Type 6613 are mounted in indicator passages. These passages should be machined directly into the engine head according to the information supplied on the sensor data sheet. For an accurate determination of peak pressure and high frequency measurements, e. g. for knock detection, the passage length should be less than 30 mm with a diameter of 5 mm.

References

[1] Bergh H., Tijdeman H., 1965, "*Theoretical and Experimental Results for the Dynamic Response of Pressure Measuring Systems,*" Technical Report NLR-TR F.238, National Aero- and Astronautical Research Institute, The Netherlands

[2] Junger M., 1997, "*Handbook of the Acoustic Characteristics of Turbomachinery Cavities,*" Editors. Lucas L., Noreen A., Sutherland C., Junger M., ASME Press, ISBN 0-7918-0054-7

[3] Schnepf M., 1998, "*Investigation of the Acoustic Resonances of Different Indicator Passages with Kistler Piezoelectric Sensors,*" Diploma Thesis, University of Applied Sciences Winterthur, Switzerland (in German)

[4] Planta J., 2000, "*Investigation of the Dynamic Properties of Sensors and Indicator Passages in a Shock Tube and in the Combustion Chamber of a Diesel Engine,*" Diploma Thesis, University of Applied Sciences Winterthur, Switzerland (in German)

[5] Walter T., Brechbühl S, Gossweiler C., Schnepf M., Wolfer P., 2004, "*Pressure Indicating with Measuring Spark Plugs on DI-Gasoline Engine – State of Technology,*" Kistler Special Print 920-333e-09.04. 2004, www.kistler.com

Kistler worldwide

Europe

Germany
Kistler Instrumente GmbH
Daimlerstrasse 6
DE-73760 Ostfildern
Tel. +49 711 34 07 0
Fax +49 711 34 07 159
info.de@kistler.com

France
Kistler France
ZA de Courtabœuf 1
15, avenue du Hoggar
FR-91953 Les Ulis cedex
Tel. +33 1 69 18 81 81
Fax +33 1 69 18 81 89
info.fr@kistler.com

Switzerland/Liechtenstein
Kistler Instrumente AG
Verkauf Schweiz
Eulachstr. 22
CH-8408 Winterthur
Tel. +41 52 224 12 32
Fax +41 52 224 14 21
sales.ch@kistler.com

Austria
Kistler GmbH
Lemböckgasse 49f
AT-1230 Wien
Tel. +43 1 867 48 67 0
Fax +43 1 867 48 67 17
sales.at@kistler.com

Italy
Kistler Italia s.r.l.
Via Ruggero di Lauria, 12/B
IT-20149 Milano
Tel. +39 02 481 27 51
Fax +39 02 481 28 21
sales.it@kistler.com

United Kingdom
Kistler Instruments Ltd.
13 Murrell Green Business Park
London Road
Hook, Hampshire RG27 9GR
Tel. +44 1256 74 15 50
Fax +44 1256 74 15 51
sales.uk@kistler.com

Denmark/Finland/Norway/Sweden
Kistler Nordic AB
Aminogatan 34
SE-431 53 Mölndal
Tel. +46 31 871 566
Fax +46 31 871 597
info.se@kistler.com

Netherlands
Kistler B.V. Nederland
Leeghwaterstraat 25
NL-2811 DT Reeuwijk
Tel. +31 182 304 444
Fax +31 182 304 777
sales.nl@kistler.com

Asia

Japan
Kistler Japan Co., Ltd.
23rd floor, New Pier Takeshiba North Tower
1-11-1, Kaigan, Minato-ku
Tokyo 105-0022
Tel. +81 3 3578 0271
Fax +81 3 3578 0278
sales.jp@kistler.com

China, People's Republic of
Kistler China Ltd.
Room 925, Yuan Chen Xin Building
No. 12 E1, Yuminlu Road Deshengmenwai
Beijing 100029
Tel. +86 10 8225 2163
Fax +86 10 8225 2124
sales.cn@kistler.com

India
Kistler Instruments (Pte) Ltd.
India Liaison Office
2B Century Plaza
560/562 Anna Salai
Teynampet, Chennai 600 018
Tel. +91 44 4213 2089
Fax +91 44 4213 2331
sales.in@kistler.com

Korea, Republic of
Kistler Korea Co., Ltd.
Gyeonggi Venture Anyang
Technical College Center 801
572-5, Anyang-Dong, Manan-Gu,
Anyang-City, Gyeonggi-Do 430-731
Tel. +82 31 465 6013
Fax +82 31 441 6015
sales.kr@kistler.com

Singapore
Kistler Instruments (Pte) Ltd.
50 Bukit Batok Street 23
#04-06 Midview Building
Singapore 659578
Tel. +65 6316 7331
Fax +65 6316 7332
sales.sg@kistler.com

Taiwan
Kistler Representative Office in Taiwan
Room 9, 8F, No. 6, Lane 180
Sec. 6, Mincyuan E. Road
Taipei 114
Tel. +886 2 7721 2121
Fax +886 2 7721 2112
sales.tw@kistler.com

Thailand
Kistler Instrument (Thailand) Co. Ltd.
662/43-46 Rama III Road
Bangpongpang, Yannawa
Bangkok 10120
Tel. +66 2293 0221-2
Fax +66 2293 0223
sales.thai@kistler.com

America

USA/Canada/Mexico
Kistler Instrument Corp.
75 John Glenn Drive
Amherst, NY 14228-2171
Tel. +1 716 691 5100
Fax +1 716 691 5226
sales.us@kistler.com

Other countries

Kistler Instrumente AG
Export Sales
Eulachstr. 22
CH-8408 Winterthur
Tel. +41 52 224 11 11
Fax +41 52 224 15 49
sales.export@kistler.com

www.kistler.com

Headquarters

Switzerland
Kistler Instrumente AG
Eulachstrasse 22, CH-8408 Winterthur
Tel. +41 52 224 11 11
Fax +41 52 224 14 14
info@kistler.com

920-352e-02.07 Mat1000 ©2007, Kistler Instrumente AG

KISTLER

measure. analyze. innovate.